1996

# Anomalous Codeposition of Fe-Ni Alloys and Fe-Ni-$SiO_2$ Composites under Potentiostatic Conditions

M. Ramasubramanian
*University of South Carolina - Columbia*

S. N. Popova
*University of South Carolina - Columbia*

Branko N. Popov
*University of South Carolina - Columbia*, popov@engr.sc.edu

Ralph E. White
*University of South Carolina - Columbia*, white@cec.sc.edu

K. M. Yin
*Yuan-Ze Institute of Technology, Taiwan*



## Publication Info

*Journal of the Electrochemical Society*, 1996, pages 2164-2172.

Publisher's link: http://dx.doi.org/10.1149/1.1836976
DOI: 10.1149/1.1836976

15. J. L. Weiniger and M. W. Breiter, *ibid.*, **111,** 707 (1964).
16. P. Oliva, X. Leonardi, J. F. Laurent, C. Delmas, J. J. Braconnier, M. Figlarz, F. Fievet, and A. de Guibert, *J. Power Sources*, **8,** 229 (1982).
17. P. V. Kamath, M. Dixit, L. Indira, A. K. Shukla, V. G. Kumar, and N. Munichandraiah, *This Journal,* **141,** 2956 (1994).
18. R. D. Armstrong and H. Wang, *Electrochim. Acta,* **36,** 759 (1991).
19. J. F. Wolf, L-S. R. Yeh, and A. Damjanovic, *Electrochim. Acta,* **26,** 759 (1981).
20. M. A. Sattar and B. E. Conway, *ibid.*, **14,** 695 (1969).
21. R. S. S. Guzmán, J. R. Vilche, and A. J. Arvía, *This Journal,* **125,** 125 (1978).
22. B. Barnard, C. F. Randell, and F. L. Tye, *J. Appl. Electrochem.*, **10,** 109, 127 (1980).
23. B. E. Conway, M. A. Sattar, and D. Gilory, *Electrochim. Acta,* **14,** 677 (1969).
24. P. W. T. Lu and S. Srinivasan, *This Journal,* **125,** 1416 (1978).
25. R. E. White, J. O'M. Bockris, and B. E. Conway, *Modern Aspects of Electrochemistry,* No. 21, p. 47, Plenum Press, New York (1990).
26. B. J. Hwang, D. T. Shieh, and A. S. T. Chang, *J. ChIChE,* **25,** 127 (1994).
27. D. T. Shieh and B. J. Hwang, *ibid.*, **25,** 87 (1994).

# Anomalous Codeposition of Fe-Ni Alloys and Fe-Ni-$SiO_2$ Composites under Potentiostatic Conditions

## Experimental Study and Mathematical Model

**M. Ramasubramanian,* S. N. Popova, B. N. Popov,** and R. E. White****

*Department of Chemical Engineering, University of South Carolina, Columbia, South Carolina 29208, USA*

**K.-M. Yin**

*Department of Chemical Engineering, Yuan-Ze Institute of Technology, Neili, Taoyuan, 32026, Taiwan*

ABSTRACT

A mathematical model has been developed to describe the electrodeposition of Fe-Ni alloys and Fe-Ni-$SiO_2$ composites under potentiostatic conditions. This model can be used to predict the polarization behavior, partial current densities, and alloy composition of each of the components as a function of the applied potential. Fe-Ni-$SiO_2$ samples were deposited on platinum rotating disk electrodes from sulfate electrolytes under potentiostatic conditions, and the results obtained were compared to the model. The model predictions were found to agree well with the experimental observations for the Fe-Ni and Fe-Ni-$SiO_2$ systems.

### Introduction

Fe-Ni deposition is classified as anomalous. Under most operating conditions, the less noble iron has a much higher deposition rate than nickel. According to Dahms[1] and Dahms and Croll,[2] Fe-Ni anomalous codeposition is due to the local pH rise at the interface due to the hydrogen evolution reaction. According to these authors, the preferential precipitation of iron hydroxide compared to nickel hydroxide causes the inhibition of nickel deposition. Romankiw and Croll[3] suggested that a trace amount of $Fe^{+3}$ in the solution causes precipitation of $Fe(OH)_3$, and that such a film accounts for the selective discharge. Nicol and Philip[4] and Swathirajan[5] attributed the underpotential deposition to the appearance of an iron dominant intermetallic compound. The importance of metal hydroxide ions in the iron plating system was suggested by Bockris *et al.*[6] They suggested that the reduction of adsorbed $Fe(OH)^+$ is the rate determining step for iron deposition. Matulis and Slizys[7] also suggested that single nickel plating goes through the formation of $Ni(OH)^+$ ions.

Recent mathematical models[8-10] that have been proposed in order to explain the phenomena of anomalous codeposition include those by Hessami and Tobias,[8] Grande and Talbot,[9] and Matlosz.[10] Hessami and Tobias[8] assumed that the electrodeposition of Fe-Ni occurs as a result of the reduction of both the bivalent metal ions, $Ni^{+2}$ and $Fe^{+2}$, and the monohydroxide ions $Fe(OH)^+$ and $Ni(OH)^+$. According to this model, the dominant mechanism in the electrodeposition process was the reduction of bivalent metal ions rather than the monohydroxide species. This is contrary to the mechanism of single-metal deposition of iron suggested by Bockris *et al.*[6] and that of nickel by Matulis and Slizys.[7]

Grande and Talbot[9] proposed a one-dimensional diffusion model in which they determined the effect of buffering and the hydrolysis reactions on predicted surface pH and deposit composition. Their model includes the assumption that anomalous deposition of nickel and iron occurs due to the electrodeposition of their respective monohydroxide species. Matlosz[10] presented a mechanism in which the codeposition reaction occurs via two step reaction mechanisms in which the monovalent intermediate ions are adsorbed on the surface of the electrode and subsequently reduced. The inhibition of nickel is assumed to be caused by the preferential adsorption of the iron intermediate over that of nickel. This competitive adsorption model was used to determine a mechanism for explaining the anomalous codeposition of Fe-Ni in terms of single metal electrodeposition in the absence of hydrogen.

One objective of the present work is to develop a mathematical model for electrodeposition of Fe-Ni alloy under potentiostatic conditions which includes material balance equations within the diffusion layer and adsorption of metal monohydroxide ions on the electrode surface. An attempt was made to determine the applicability of the model to our experimental data obtained by electrodeposition of Fe-Ni alloy under potentiostatic conditions from sulfate electrolytes. The monohydroxide ions $Fe(OH)^+$ and $Ni(OH)^+$ are assumed to undergo an adsorption-reduction mechanism. The rate of discharge of $Fe(OH)^+$ and $Ni(OH)^+$ are proportional to their respective surface coverage fractions. Electrodeposition occurs due to the discharge of monohydroxide species only and not from the direct reduction of bivalent ions.

* Electrochemical Society Student Member.
** Electrochemical Society Active Member.

A second objective of this work was to evaluate experimentally the effect of $SiO_2$ colloidal particles on the electrodeposition of iron-nickel alloy and to develop a mathematical model for electrodeposition of iron-nickel alloys in the presence of $SiO_2$ colloidal particles which takes into account iron-nickel plating bath solution chemistry, mass transfer, and surface reactions.

The model presented here gives, in addition to the partial current densities of the various reactions, the amount of inert particles incorporated during the deposition of Fe-Ni-$SiO_2$ alloys from sulfate electrolytes. An attempt was also made to determine the applicability of the model to our experimental data obtained under potentiostatic conditions. The inclusion of $SiO_2$ in the deposit is modeled using Guglielmi's[11] assumptions for a codeposition mechanism which includes two successive adsorption steps: loose adsorption and subsequent strong adsorption of inert particles.

## Experimental

In order to use the experimental data to model Fe-Ni electrodeposition, rotating disk electrodes of exposed area of 0.458 $cm^2$ at a constant rotation speed of 200 rpm were used for the electrodeposition of Fe-Ni alloys. The deposits for Fe-Ni alloys were obtained from a bath containing 0.5 *M* $NiSO_4$, 0.1 *M* $FeSO_4$, and 0.5 *M* $Na_2SO_4$. 0.1 *M* of boric acid was added as buffer, and the pH of the solution was adjusted to 3.0 by adding 20% $H_2SO_4$. The deposited alloys were dissolved in 50% $HNO_3$ and 50% HCl solution, then diluted and nickel and iron content of the alloy was determined using an atomic absorption spectrometer (AA). The side reaction of hydrogen evolution was determined by subtraction of the partial current density of nickel and iron from the total current density. Identical deposition conditions were maintained throughout the duration of each electrodeposition.

Rotating disk electrodes of exposed area of 0.458 $cm^2$ were also used to deposit Fe-Ni-$SiO_2$ alloys. The plated alloys were stripped and analyzed for iron and nickel content using AA. The partial current densities of hydrogen reduction were determined by subtracting the partial current densities of Ni and Fe from the total current during electrodeposition. However, deposition of Fe-Ni-$SiO_2$ carried out on the demountable rotating disk electrodes did not produce any analytically measurable amount of inert particles in the deposit. Thus, in order to obtain the weight fraction of inert particles that are included in the deposit, electrodeposition of Fe-Ni-$SiO_2$ alloy was carried out on a square platinum electrode with an exposed area of 7.5 $cm^2$ in a well-stirred bath. The particle size of $SiO_2$ used in this study was in the range of 30 to 50 μm (Aldrich Chemical Company) with a density of 2.2 $g/cm^3$. The electrolyte was stirred during this experiment to simulate the conditions for the rotating disk electrode. Van Camp,[12] by using a mass transfer analysis for rotating disk electrodes, showed that a minimum stirring rate is essential for keeping the inert particles in suspension. These results were verified by Rajiv *et al.*,[13] who determined the effect of the bath parameters such as the concentration of the dispersoid, $SiO_2$ in our case, current density, pH, stirring rate, surfactants, and chloride ion concentration for their cobalt-titania codeposition system approximating the rotating disk conditions by using a magnetic stirring apparatus.

The Fe-Ni-$SiO_2$ deposits were obtained from a bath containing 0.5 *M* $NiSO_4$, 0.1 *M* $FeSO_4$, and 0.5 *M* $Na_2SO_4$ and various concentrations of colloidal $SiO_2$. Boric acid (0.1 *M*) was added as a buffer, and the pH of the solution was adjusted to 3.0 by adding 20% $H_2SO_4$. Platinum gauze was used as the anode. The deposition potential was controlled by a potentiostat/galvanostat (EG&G 273) using standard calomel electrode (SCE) as a reference electrode. The corresponding current density throughout the deposition was monitored. The deposition was carried out for half an hour, and the deposits were cleaned, dried, and weighed. The amount of alloy deposited was determined by the difference in weight. Electrodeposition was carried out at constant potentials from −1.0 to −1.5 V in intervals of 0.1 V *vs.* SCE. The electrodeposited alloy samples were then dissolved in a solution of 50% $HNO_3$ and 50% HCl. The solutions were then made up to 50 ml and subjected to analysis by titrimetric methods. The following procedure was applied to all samples:[14] (*i*) 25 ml of the sample was taken and diluted with distilled water; (*ii*) 5 ml of 1:1 $HNO_3$ was added and the solution was boiled for 5 min; and (*iii*) excess amount of $NH_4Cl$ salt was added to this solution and boiled again. A strong alkaline reaction was obtained by adding 1:1 ammonia solution to the sample. The solution was again boiled to coagulation. Next, the precipitate was filtered and washed. The filtrate contained all the nickel, and the precipitate constituted the iron components. Thus the iron and nickel were separated and were ready for analytical determination. The amount of $SiO_2$ in the deposit was calculated by subtraction of the weight of nickel and iron from the total weight of deposited alloy.

*Analysis for nickel.*—The filtrate was taken in an Erlenmeyer flask and Murexide indicator was added until the solution turned light brown in color. The solution then was titrated against 0.01 *M* ethylenediaminetetraacetic acid (EDTA) solution. The end point was the change of color from light brown to purple. The amount of nickel was determined using the equation: weight of Ni = ml of 0.01 *M* EDTA × 0.5869.

*Analysis for iron.*—The precipitate obtained during the separation process was dissolved with hot dilute $HNO_3$ and diluted with distilled water. The solution pH was adjusted between 1.5 and 2.0 by adding ammonia. The resulting mixture was heated to 40°C and (after addition of 2 ml of sulfosalicylic acid indicator) was titrated against 0.01 *M* EDTA solution. The color change was from a deep pink to pale yellow or colorless. The amount of iron present in the solution was determined by using the correlation: weight of Fe = ml of 0.01 *M* EDTA × 0.5585. The partial current densities of iron and nickel deposition were then calculated assuming Faraday's law. The amount of $SiO_2$ incorporated in the deposit was determined by difference in weight of the sample after deducting the amount of iron and nickel deposited.

Experiments were performed in triplicate, and the average values were reported.

## Model Development

*Mathematical model for the codeposition of Fe-Ni alloy.*—The first step in developing a mathematical model for the codeposition of Fe-Ni-$SiO_2$ alloys is to determine a set of equations describing the Fe-Ni system. The experimental data obtained for Fe-Ni codeposition as described above were compared to the solution obtained from solving the set of equations suggested by Hessami and Tobias.[8] According to the equations in their model, the calculation of concentrations of the respective ionic species show that, at higher overpotentials, the concentrations of $Fe(OH)^+$ and $Ni(OH)^+$ decrease at the electrode surface. Thus, at higher overvoltages, the partial current densities due to the reduction of the monovalent ions $Fe(OH)^+$ and $Ni(OH)^+$ are relatively small when compared to the current densities obtained from the electrochemical reduction of the bivalent ions. This suggests that the electrodeposition occurs primarily through the reduction of bivalent $Ni^{+2}$ and $Fe^{+2}$ ions which is in contradiction to Bockris *et al.*[6] and Matulis and Slizys[7] for single ion deposition and also contradicts Hessami and Tobias's[8] assumption that charge transfer of $Fe(OH)^+$ and $Ni(OH)^+$ species is responsible for anomalous codeposition of Fe-Ni alloys. Moreover, experiments carried out in this study for the electrodeposition of Fe-Ni from electrolytes containing 0.5 *M* $Ni^{+2}$ and 0.1 *M* $Fe^{+2}$ and their subsequent analysis showed that the partial current densities observed for iron are always higher than that of nickel. The predicted nickel partial current density is much higher than that of iron. This results from the coupling of two nickel formation reactions, *i.e.*, reduction of

its monohydroxide ion and that of the bivalent $Ni^{+2}$ ion, which has a higher exchange current density and lower deposition potential than iron.

In order to explain the anomalous codeposition of Fe-Ni under potentiostatic conditions we propose the following model: (*i*) electrodeposition occurs solely due to the reduction of the metal-hydroxide ions ($Ni(OH)^+$ and $Fe(OH)^+$) and not by direct two-electron transfer to the metal ions ($Fe^{+2}$ and $Ni^{+2}$). (*ii*) The electrode surface is assumed to be fully covered by the metal hydroxide ions, the coverage being defined as $\theta_{NiOH^+}$ and $\theta_{FeOH^+}$. (*iii*) The exchange current densities of the reactions involving the reduction of monohydroxide ions depend on the concentration of the respective metal hydroxide ion[15] and the pH near the electrode surface.

The model proposed here was developed to predict the effect of various plating parameters such as bulk pH, concentration of the respective ions in the bulk, etc., on the resulting alloy composition and current efficiency. The model includes mass transfer, adsorption, and electrochemical reactions. The equations are written for a rotating disk electrode system. Mass transfer is governed by convection, diffusion, and migration, and the kinetics of the electrochemical reactions are governed by Butler-Volmer equations. Dilute solution theory[16] applies and steady-state conditions are assumed.

*Reactions.*—The following electrochemical reactions are assumed to occur at the surface of the electrode

$$Ni(OH)^+ + 2e^- \rightarrow Ni + OH^- \quad [1]$$

$$Fe(OH)^+ + 2e^- \rightarrow Fe + OH^- \quad [2]$$

$$2H^+ + 2e^- \rightarrow H_2 \quad [3]$$

The homogeneous equilibrium reactions which are assumed to occur in this system are

$$Ni^{2+} + OH^- \rightleftarrows Ni(OH)^+ \quad [4]$$

$$Fe^{2+} + OH^- \rightleftarrows Fe(OH)^+ \quad [5]$$

$$H^+ + SO_4^{2-} \rightleftarrows HSO_4^- \quad [6]$$

$$H^+ + OH^- \rightleftarrows H_2O \quad [7]$$

*Equations.*—The general material balance equations for a species i is given by

$$\frac{\partial c_i}{\partial t} = -\nabla \cdot N_i + R_i \quad [8]$$

where $R_i$ denotes the rate of production of species i in solution from a homogeneous reaction and $N_i$ is the flux including migration, diffusion, and convection and is given as[16]

$$N_i = -\frac{z_i D_i F c_i}{RT}\frac{d\Phi}{dy} - D_i\frac{dc_i}{dy} + v_y c_i \quad [9]$$

The expression of convection by moderate stirring, *i.e.*, $v_y$ is not easy to express in a quantitative way. Thus a velocity profile from the rotating disk electrode system was chosen for this study. A moderate rotation speed of 200 rpm was specified. By algebraic manipulations of the individual species material balances to remove the $R_i$ terms, the following equations are obtained

$$-\nabla \cdot N_{Ni^{+2}} - \nabla \cdot N_{NiOH^+} = 0 \quad [10]$$

$$-\nabla \cdot N_{Fe^{+2}} - \nabla \cdot N_{FeOH^+} = 0 \quad [11]$$

$$-\nabla \cdot N_{SO_4^{-2}} - \nabla \cdot N_{HSO_4^-} = 0 \quad [12]$$

$$-\nabla \cdot N_{H^+} + \nabla \cdot N_{OH^-} - \nabla \cdot N_{Ni^{+2}} - \nabla \cdot N_{Fe^{+2}} - \nabla \cdot N_{HSO_4^-} = 0 \quad [13]$$

$$-\nabla \cdot N_{Na^+} = 0 \quad [14]$$

Equations 10-14 are the result of the overall material balances on nickel, iron, sulfate, hydrogen, and sodium ions, respectively. The equilibrium equations for the components in solution constitute the following equations

$$c_{Ni^{+2}}c_{OH^-} - K_1 c_{NiOH^+} = 0 \quad [15]$$

$$c_{Fe^{+2}}c_{OH^-} - K_2 c_{FeOH^+} = 0 \quad [16]$$

$$c_{H^+}c_{OH^-} - K_3 = 0 \quad [17]$$

$$c_{H^+}c_{SO_4^{-2}} - K_4 c_{HSO_4^-} = 0 \quad [18]$$

where $K_1$, $K_2$, $K_3$, and $K_4$ are the equilibrium constants for their respective reactions. The electroneutrality condition is

$$\sum z_i c_i = 0 \quad [19]$$

*Boundary conditions.*—At the boundary denoting $y = \delta$, all concentrations are equal to their bulk values

$$c_i = c_i^{bulk} \quad [20]$$

The bulk equilibrium conditions are described by Eq. 15-18. At the electrode surface, $y = 0$, for the nine ionic species at the interface, the flux equations can be written as[16]

$$\frac{z_i D_i F c_i}{RT}\left(\frac{\partial \Phi}{\partial y}\right) + D_i\left(\frac{\partial c_i}{\partial y}\right) - \sum_{j=1}^{nr}\left(\frac{s_{i,j} i_j}{n_j F}\right) = 0 \quad [21]$$

where $s_{i,j}$ is the stoichiometric coefficient in the electrochemical reaction j where the reaction is expressed as

$$\sum_i s_{i,j} M_i^{z_i} \rightarrow n_j e^- \quad [22]$$

The partial current density of each reaction j obeys Butler-Volmer kinetics. Due to the surface adsorption phenomena, the expressions given below for current density are modified according to the following assumptions: (*i*) the discharge rates of $Fe(OH)^+$ and $Ni(OH)^+$ are proportional to the fraction of the surface covered by them, and (*ii*) the species adsorption fractions are related to their respective interfacial concentrations and are governed by the Langmuir isotherm. Thus, the modified Butler-Volmer equation for the nickel deposition can be written in the following form

$$i_1 = i_{o1}\theta_{NiOH^+}\left\{\exp\left(\frac{\alpha_{a_1} F\eta_{1,ref}}{RT}\right) - \frac{c_{NiOH^+,o}}{c_{NiOH^+,bulk}}\exp\left(\frac{-\alpha_{c_1} F\eta_{1,ref}}{RT}\right)\right\} \quad [23]$$

where $i_{o1}$ is the exchange current density for $Ni(OH)^+$ reduction, which depends on the concentration of $Ni(OH)^+$ ions at the surface.

Similiarly

$$i_2 = i_{o2}\theta_{FeOH^+}\left\{\exp\left(\frac{\alpha_{a_2} F\eta_{2,ref}}{RT}\right) - \frac{c_{FeOH^+,o}}{c_{FeOH^+,bulk}}\exp\left(\frac{-\alpha_{c_2} F\eta_{2,ref}}{RT}\right)\right\} \quad [24]$$

$$i_3 = i_{o3}\left\{\exp\left(\frac{\alpha_{a_3} F\eta_{3,ref}}{RT}\right) - \frac{c_{H^+,o}}{c_{H^+,bulk}}\exp\left(\frac{-\alpha_{c3} F\eta_{3,ref}}{RT}\right)\right\} \quad [25]$$

where $\eta_{j,ref} = V_d - \Phi_0 - E_{e,j}$. The surface coverage of $FeOH^+$ and $NiOH^+$ are given as

$$\theta_{NiOH^+} = \frac{c_{NiOH^+,o}}{c_{NiOH^+,o} + c_{FeOH^+,o}} \quad [26]$$

$$\theta_{FeOH^+} = 1 - \theta_{NiOH^+} \quad [27]$$

*Development of equations describing the codeposition of inert particles.*—Several possible mechanisms have been

suggested in the literature to explain particle codeposition: (*i*) electrophoresis proposed by Whithers,[18] (*ii*) mechanical entrapment suggested by Martin and Williams,[19] and (*iii*) adsorption of particles suggested by Brandes and Golthorpe.[20] Also a mathematical expression was suggested by Kariapper and Foster[21] which describes the effect of hydrodynamics. Celis *et al.*[22] proposed a model starting from a statistical approach. Valdes[23] developed a model by assuming a Butler-Volmer-type kinetic expression for the deposition of colloidal particles, and by considering the inert particle flux onto the electrode surface to be due to diffusion and convection. Fransaer *et al.*[24] derived expressions for the codeposition of metals based on an analysis of the different forces acting on an inert particle.

The model proposed for the electrodeposition of Fe-Ni alloys is based on the occurrence of electrodeposition through the adsorption and subsequent reduction of metal monohydroxide ions, $FeOH^+$ and $NiOH^+$. These ions are assumed to adsorb on the surface of the electrode according to a Langmuir-type adsorption isotherm. Based on the similarity between a plot of volume percent of codeposited particles in the deposit and volume percent of inert particles in the solution to the Langmuir adsorption isotherm curve, Guglielmi[11] postulated a mechanism based on two successive adsorption steps. The first step consists of a loose adsorption ($\theta_{SiO_2}$) physical in nature resulting in a high degree of adsorption. A subsequent field-assisted strong adsorption causes the entrapment of particles in the metal layer. In the case of Fe-Ni-$SiO_2$ electrodeposition, the three species, $FeOH^+$, $NiOH^+$, and $SiO_2$ will compete for adsorption sites on the electrode surface.

The volume of $SiO_2$ included per unit area per unit time $dv_{SiO_2}/dt$ can be related to the coverage of inert particles on the electrode surface by the equation developed by Guglielmi[11]

$$\frac{dv_{SiO_2}}{dt} = \theta_{SiO_2} v_o e^{BE} \qquad [28]$$

where $v_o$ is a constant which is a measure of the factor of inclusion caused by adsorption of inert particles onto the surface. $B$ is a constant which determines the factor of inclusion controlled by the applied potential, $E$. The amount of inert particles incorporated in the deposit can be determined by estimating $B$ and $v_o$ from experimental data. This can be done by correlating the amount of included inert particles as a function of the amount of electrodeposited alloy. A volume fraction of $SiO_2$ ($\alpha_{SiO_2}$) is defined as the ratio of volume of the inert particles imbedded in the alloy to the total volume of alloy and $SiO_2$ deposited

$$\alpha_{SiO_2} = \frac{dv_{SiO_2}}{dt} \Big/ \frac{dv_m}{dt(1 - \alpha_{SiO_2})} \qquad [29]$$

where $dv_m/dt(1 - \alpha)$ is the differential amount of metal + inert particles deposited during a small time interval. The value of $dv_m/dt$, the amount of metal ions deposited at any instant, is determined by Faraday's laws as

$$\frac{dv_m}{dt} = \sum_k \sum_j \frac{i_j w_{k,j}}{n_j F d_{k,j}} \qquad [30]$$

where $w_{k,j}$ is the atomic weight of the metal k deposited in reaction j, $n_j$ is the number of electrons involved in the reaction j, $F$ is the Faraday's constant, and $d_{k,j}$ is the density of metal k in reaction j.

For the Fe-Ni-$SiO_2$ system, the volume fraction of $SiO_2$ in the deposit can be determined if one estimates the values of partial current densities of metal deposition ($i_{NiOH^+}$, $i_{FeOH^+}$), the surface coverage of inert particles ($\theta_{SiO_2}$), and the constants $v_0$ and $B$. The constants $v_0$ and $B$ can be estimated by determining the amount of $SiO_2$ and the metal deposited under various concentrations and applied potentials. Substituting Eq. 28 and 30 in 29 and rearranging, one obtains the volume fraction of inert particles deposited as

$$\frac{\alpha_{SiO_2}}{(1 - \alpha_{SiO_2})} = \theta_{SiO_2} v_o e^{BE} \left[ \sum_k \sum_j \frac{i_j w_{k,j}}{n_j F d_{k,j}} \right]^{-1} \qquad [31]$$

where the summation terms indicate the number of metals deposited, $k$, and the number of the electrochemical reactions, $j$, involved. Equation 31 can then be used to determine the amount of $SiO_2$ incorporated at the electrode.

## Solution Procedure

The potentiostatic model developed for the Fe-Ni deposition process without $SiO_2$ can be used to predict the partial current densities of iron and nickel electrodeposition based on the reduction of $NiOH^+$ and $FeOH^+$ ions. The volume fraction of inert particles in the electrodeposit can be found by simultaneously solving the set of equations described in the modeling of Fe-Ni electrodeposition along with the equation describing the inert particle inclusion (Eq. 31). The only modification that has to be done in the model for Fe-Ni is that of the equations of surface coverage. Incorporating the coverage of $SiO_2$ in the Langmuir-type equations for $NiOH^+$ and $FeOH^+$ (Eq. 26 and 27), the modified Langmuir isotherm at the electrode surface is given by

$$\theta_{NiOH^+} = \frac{c_{NiOH^+,o}}{c_{NiOH^+,o} + c_{FeOH^+,o} + k_{SiO_2} c_{SiO_2}} \qquad [32]$$

$$\theta_{FeOH^+} = \frac{c_{FeOH^+,o}}{c_{NiOH^+,o} + c_{FeOH^+,o} + k_{SiO_2} c_{SiO_2}} \qquad [33]$$

where $k_{SiO_2}$ is the ratio of the adsorption equilibrium constants of $SiO_2$ and the metal hydroxide ions. The surface coverage due to $SiO_2$ is then

$$\theta_{SiO_2} = 1 - \theta_{NiOH^+} - \theta_{FeOH^+} \qquad [34]$$

The above system of equations was then solved iteratively in order to determine the unknown concentrations, $\theta_{NiOH^+}$, $\theta_{FeOH^+}$, and $\alpha_{SiO_2}$. A three-point finite difference procedure was used, and the resulting expressions were solved using the Newman's BAND(J) subroutine.[16,17] Central differences were used in the solution domain and backward and forward differences were used at $y = 0$ and $y = \delta$, respectively.

*Model parameters.*—The kinetic parameters used for the electrochemical reactions are given in Table I. The equilibrium constant values used are given in Table II. The mass transfer and concentration data are given in Table III. The other parameters, namely, the constants $k_{SiO_2}$, $v_0$, and $B$ were estimated using the minimization of

**Table I.**

| Reactions | $\alpha_{a,j}$[a] | $\alpha_{c,j}$[b] | $\eta_j$ | $E_{e,j}$ (V) | $i_{0j}$ (A/cm$^2$)[e] |
|---|---|---|---|---|---|
| 1 | 1.5 | 0.5 | 2 | −0.3585[c] | $0.2973 \times 10^{-4}$ |
| 2 | 1.5 | 0.5 | 2 | −0.654[d] | $0.3848 \times 10^{-2}$ |
| 3 | 1.5 | 0.5 | 2 | 0.0 | $0.6063 \times 10^{-3}$ |

[a] $n_j - \alpha_{c,j}$.
[b] Ref. 30.
[c] Derived according to Newman[16]: $FE_{e,Ni/NiOH^+} - FE_{e,Ni/Ni^{+2}} = 1/2\ RT \ln (\lambda_{NiOH^+}/\lambda_{Ni^{+2}}\lambda_{OH^-})$.
[d] Derived according to Newman[16]: $FE_{e,Fe/NiOH^+} - FE_{e,Fe/Ni^{+2}} = 1/2\ RT \ln (\lambda_{FeOH^+}/\lambda_{Fe^{+2}}\lambda_{OH^-})$.
[e] Estimated using Eq. 35.

**Table II.**

| $i$ | Equilibrium constant ($K_i$) | Ref. |
|---|---|---|
| 1 | $4.5 \times 10^{-5}$ (mol/liter) | 8 |
| 2 | $5.78 \times 10^{-8}$ (mol/liter) | 8 |
| 3 | $1.2 \times 10^{-1}$ (mol/liter) | 22 |
| 4 | $1.0 \times 10^{-14}$ (mol/liter) | 22 |

**Table III.**

| Species | $z_i$ | $D_i \times 10^5$ (cm²/s) | $c_{i,bulk}$[a] (mol/cm³) |
|---|---|---|---|
| $Ni^{2+}$ | 2 | 0.72[b] | $0.5 \times 10^{-3}$ |
| $NiOH^+$ | 1 | 0.72[c] | $0.1111 \times 10^{-9}$ |
| $Fe^{+2}$ | 2 | 0.713[b] | $0.9998 \times 10^{-4}$ |
| $FeOH^+$ | 1 | 0.713[c] | $0.1730 \times 10^{-7}$ |
| $SO_4^{-2}$ | −2 | 1.06[d] | $0.1060 \times 10^{-2}$ |
| $HSO_4^-$ | −1 | 1.33[d] | $0.8152 \times 10^{-4}$ |
| $H^+$ | 1 | 0.913[d] | $1.0 \times 10^{-6}$ |
| $OH^-$ | −1 | 5.26[d] | $1.0 \times 10^{-14}$ |
| $Na^+$ | 1 | 1.334[d] | $1.0 \times 10^{-3}$ |

[a] Calculated equilibrium bulk concentrations.
[b] Ref. 28, p. 99.
[c] Chosen the same as the corresponding metal ion.
[d] Ref. 16, p. 255.

error routine DBCLSF from the IMSL Library based on the minimization of residues from the experimental and calculated data ($i_{Ni}$, $i_{Fe}$, $i_{H_2}$, $\alpha_{SiO_2}$). The experimental data obtained for deposits plated in the presence of 3 g/liter colloidal $SiO_2$ in the bath were used to estimate the values of $k_{SiO_2}$, $v_0$, $B$, and the exchange current densities of the electrochemical reactions involving the reduction of $NiOH^+$ and $FeOH^+$. The function to be minimized was given as

$$\min \sum \left( \frac{i_{j,predicted} - i_{j,experimental}}{i_{j,experimental}} \right)^2 \quad [35]$$

for the partial currents of each reaction j. A similar equation was used for the prediction using $\alpha_{SiO_2}$. The values of $k_{SiO_2}$, $B$, and $v_0$ were found to be 2.98, 0.41 $V^{-1}$, and $3.7 \times 10^{-5}$ cm/s, respectively.

## Results and Discussion

*Electrodeposition of Fe-Ni alloy.*—The bulk equilibrium solution chemistry for Fe-Ni plating bath alone has been studied by Yin *et al.*[25] The equilibrium concentrations of different species in the bulk under equilibrium conditions were calculated for the test electrolyte containing 0.5 *M* $NiSO_4$, 0.1 *M* $FeSO_4$, and 0.5 *M* $Na_2SO_4$ at a bulk pH of 3.0 and are given in Table III.

The normalized concentration profiles, expressed as $c_i/c_{i,bulk}$ of $Fe^{+2}$, $Ni^{+2}$, and $H^+$ are shown for a deposition potential of −1.4 V (*vs.* SCE) in Fig. 1. The concentration profiles of $Fe^{+2}$ and $Ni^{+2}$ show very small variation from their bulk values, since the only change in these concentrations occurs from their conversion into their respective monohydroxide species. Due to the hydrogen evolution reaction, the concentration of $H^+$ decreases as one approaches the surface of the electrode, thereby resulting in an increase in pH. The calculations from the model show that the pH increases from a value of 3.0 in the bulk to 4.37 near the surface of the electrode. As shown in Fig. 2, this increase in pH causes the concentrations of $FeOH^+$ and $NiOH^+$ to increase near the electrode surface. The normalized concentration of $FeOH^+$ and $NiOH^+$ increase by about 50 times their value at the bulk. This is consistent with the observations of Yin *et al.*[25] and Grande and Talbot[9] who showed that the concentration of the monohydroxide ions increase approximately by an order of magnitude with every unit increase in pH. Comparison of the pH values obtained from the model at the electrode surface with the solution equilibrium diagram developed by Yin *et al.*[25] showed that the pH increase near the electrode surface is not sufficient to cause the formation of the hydroxide species $Fe(OH)_2$ and $Ni(OH)_2$, and thus the assumption of neglecting these species is valid.

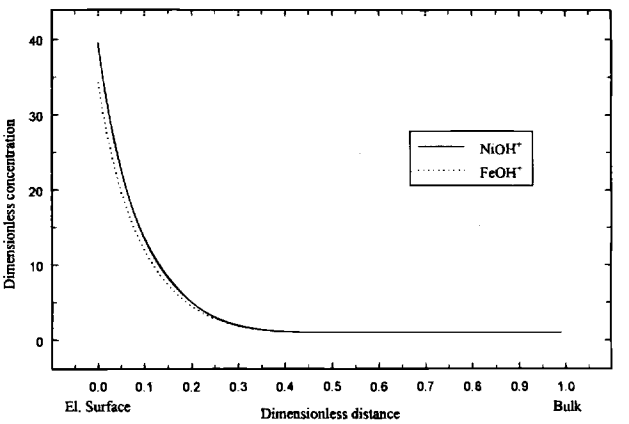


**Fig. 2. Normalized concentration profiles of $FeOH^+$ and $NiOH^+$ from the electrode surface ($y = 0$) to the bulk ($y = 1$).**

Figure 3 shows the comparison between the model predictions and the experimental results obtained for the partial current densities of Ni, Fe deposition, and $H_2$ evolution. The simulated curves agree well with the partial current densities obtained from the experiments. The experimental data obtained in this study show that the partial current densities of iron deposition are almost always greater than those of nickel, which is also predicted by the model. At low applied potentials, up to a cathode potential of −1.0 V, the predicted iron partial current density is nearly equal to the partial current density of nickel. This is due to more negative deposition potential for the $FeOH^+$ species when compared to the deposition potential of $NiOH^+$ species, which offsets the larger cur-

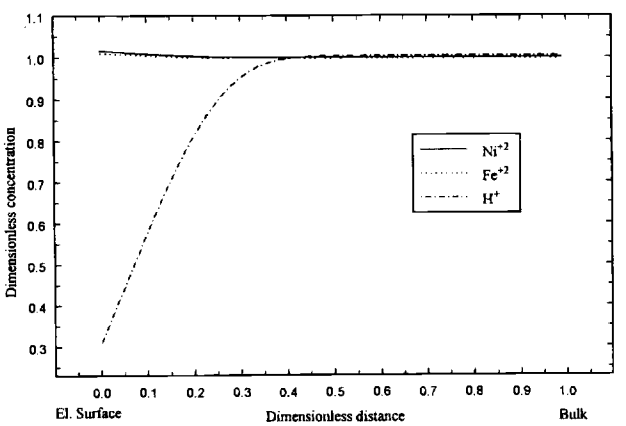


**Fig. 1. Normalized concentration profiles of $Fe^{+2}$, $Ni^{+2}$, and $H^+$ from the electrode surface ($y = 0$) to the bulk ($y = 1$).**

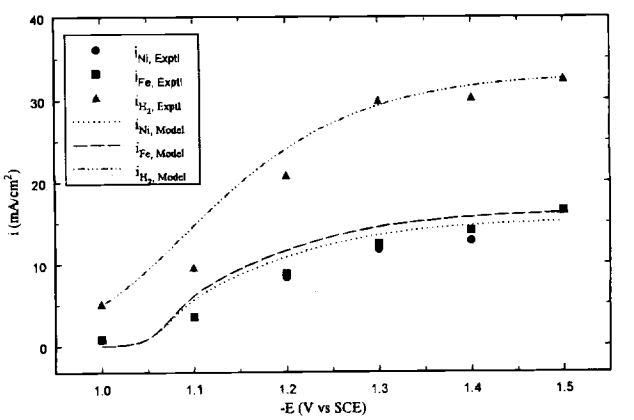


**Fig. 3. Comparison of model predictions and experimental values for the partial currents of Fe, Ni, and $H_2$.**

rents expected due to the higher concentration of $FeOH^+$ over $NiOH^+$ as predicted by the equilibrium diagram for Fe-Ni system.[25] As shown in Fig. 3, the hydrogen partial current density is higher than the iron and nickel partial current densities. At low overpotentials the hydrogen reaction is under kinetic control. Thus the hydrogen evolution current density increases by increasing the deposition potential.

The experimental data and model predictions for the weight fraction of Fe ($X_{Fe}$) in the deposit are shown in Fig. 4. The model and experimental data are in good agreement. The model prediction also shows a decrease in the composition of iron at lower overvoltages. This can be attributed to the fact that the deposition potential for nickel from $Ni(OH)^+$ is more positive than that of Fe from $Fe(OH)^+$. Thus, at lower deposition potentials, even though the concentration of $Ni(OH)^+$ is much less than $Fe(OH)^+$ a larger amount of nickel is deposited while the iron content in the alloy is negligibly small.

*Electrodeposition of Fe-Ni-$SiO_2$ alloy.*—Since the Fe-Ni alloy composition is determined by the competition of reactive species ($FeOH^+$, $NiOH^+$, and $H^+$) on the electrode surface,[7-9,25] the presence of colloidal $SiO_2$ in the electrolyte may suppress the hydrogen evolution by absorbing on the surface of the substrate and may play a significant role on the iron and nickel composition profiles. Also, inclusion of inert particles in the alloy is expected to enhance the mechanical properties of the composite.

*Linear sweep voltammetry (LSV).*—LSV was used as an *in situ* technique for studying alloy electrodeposition and dissolution in the presence and absence of inert $SiO_2$ colloidal particles in the electrolyte. LSV was applied to dissolve the alloy anodically. Platinum disks with exposed area of 0.458 $cm^2$ were used as the working electrodes; the anode used was a large platinum gauze and a SCE served as a reference electrode. The LSV curves obtained in an electrolyte containing 0.5 *M* $NiSO_4$, 0.1 *M* $FeSO_4$, and 0.5 *M* $Na_2SO_4$ in the presence of different concentrations of $SiO_2$ are shown in Fig. 5. The deposition of Fe-Ni alloy in Fig. 5 was carried out at sweep rate of $v$ = 20 mV/s. When the applied cathodic potential becomes more negative than −1.0 V *vs.* SCE, a broad current peak with an $E_{pa}$ = −0.4 V *vs.* SCE appears on the anodic branch. In Fig. 5, the alloy stripping peak decreases as the concentration of $SiO_2$ increases in the electrolyte. The amount of the charges used to deposit the alloy in the presence of $SiO_2$ was estimated by integrating the area under the anodic peak. The charge, removed, at a sweep rate of 20 mV/s and reverse potential of −1.05 V *vs.* SCE as a function of concentration of $SiO_2$, are summarized in Fig. 6. According to Fig. 6, the alloy deposition was reduced in the presence of different concentrations of $SiO_2$ up to 22%, compared with the corresponding values of charges obtained in the absence of

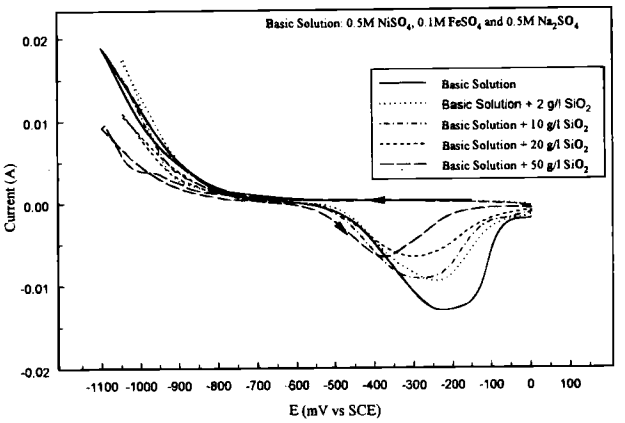


**Fig. 5. Linear sweep voltammetric (LSV) curves obtained for a solution of 0.5 *M* $NiSO_4$, 0.1 *M* $FeSO_4$, and 0.5 *M* $Na_2SO_4$ in presence of different concentrations of $SiO_2$ in solution; $v$ = 20 mV/s.**

$SiO_2$. The alloy deposition involves the adsorbate intermediates $Ni(OH)^+$ and $Fe(OH)^+$.[8,9,25] It is apparent from Fig. 6 that the participation of $SiO_2$ causes the alloy deposition rates to be inhibited. Adsorbed $SiO_2$ reduces the surface coverage of $Ni(OH)^+$ and $Fe(OH)^+$ by decreasing the active surface area for both reduction processes.

A plot of the predicted surface coverage of $SiO_2$ as a function of the potential in the presence of different concentrations of $SiO_2$ is presented in Fig. 7. As expected, at a given deposition potential, an increase in concentration of the inert particle causes more $SiO_2$ to be adsorbed on the surface, thereby increasing the surface coverage of the inert particles on the electrode. As the deposition potential is increased in the cathodic direction, the coverage of $SiO_2$ decreases. This phenomenon can be explained by taking into account that the actual number of inert particles on the electrode surface is less when compared to the number $FeOH^+$ particles. Thus, as the potential increases in the cathodic direction the number of reduced ions increases, which causes the relative concentrations of the reacting ions on the surface to change. The change in the number of $SiO_2$ particles on the electrode surface is greater than a corresponding change in $FeOH^+$ ions, thus forcing the surface coverage fraction of $SiO_2$ to decrease. Figure 8 depicts the EDS spectrum of the deposits plated at −1.2 V *vs.* SCE in the presence of different concentrations of $SiO_2$ in the electrolyte. According to this figure, significant amounts of $SiO_2$ are included in the plate deposited at −1.2 V *vs.* SCE from electrolyte containing colloidal $SiO_2$ in the range of 3 up to 100 g/liter.

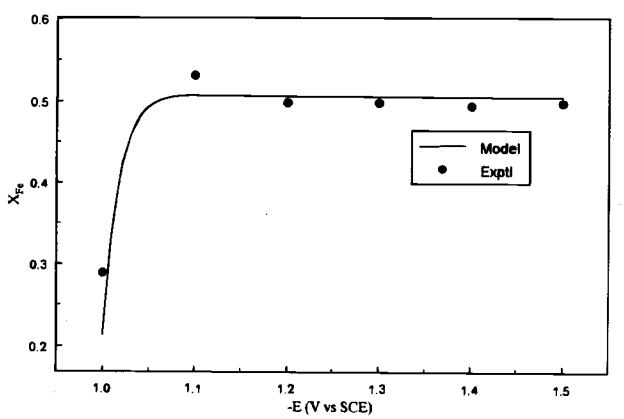


**Fig. 4. Comparison of model prediction and experimental data for the weight fraction of Fe in the deposit.**

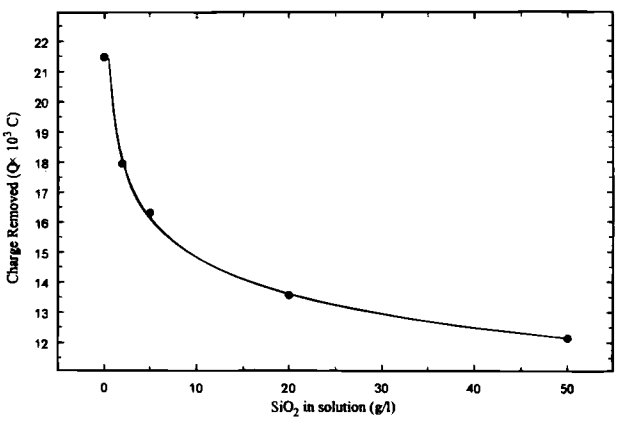


**Fig. 6. Plot of the total charge removed from the anodic sweep of cyclic voltammograms obtained at reverse potential of −1.05 V *vs.* SCE with different concentrations of $SiO_2$ in solution.**

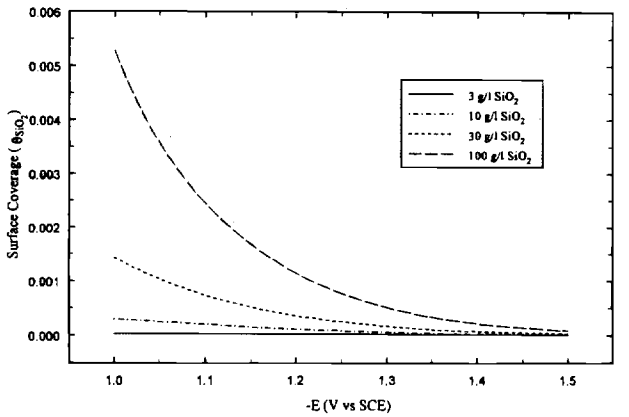


**Fig. 7. Plot of the surface coverage of $SiO_2$ as a function of potential at different concentrations of $SiO_2$ in solution.**

*Comparison of model predictions and experimental data.*—A comparison of model predictions and experimental data obtained for the partial currents of iron, nickel, and hydrogen reduced from a bath containing 3 g/liter $SiO_2$ is presented in Fig. 9. In this figure, both experimental data and model predictions show that the partial current density of iron is greater in magnitude than that of nickel. Since the experimental data obtained for deposits plated in the presence of 3 g/liter colloidal $SiO_2$ in the bath were used to estimate the values of the different parameters, the validity of the model was tested with a different set of experimental data using the values of the parameters from the previous fit. The model predictions and experimentally obtained partial current densities of nickel with different concentrations of colloidal $SiO_2$ in the electrolyte are presented in Fig. 10. There is, in general, good agreement of the simulated curves with the experimental data obtained for these electrolytes. In this plot, the reaction rate for nickel is inhibited significantly with the addition of $SiO_2$ in the electrolyte. The enhanced polarization of nickel deposition by increasing the concentration of colloidal $SiO_2$ in the electrolyte is due to blocking of the active surface sites by $SiO_2$. As the deposition potential is increased to a more cathodic value, it seems that the inhibition of nickel by increasing the amount of $SiO_2$ in solution is less effective than at a less cathodic deposition potential. This is due to the increased rate of nickel electrodeposition which produces a more active area for the metal deposition than at lower overpotentials. The electrode area is blocked by $SiO_2$ particles and by the electrodepositing ions; thus, a larger deposition rate means a larger available area for the ions to adsorb on the available sites created by the previously adsorbed ion. Accordingly, the effect of the area blocked by $SiO_2$ at higher cathodic deposition potentials is considerably less than at lower deposition potentials.

A similar plot for the partial current densities of Fe at different concentrations of colloidal $SiO_2$ in the electrolyte, is given in Fig. 11. It can be inferred from Fig. 10 and 11 that the magnitude decrease in partial current densities is smaller for iron compared to nickel. This can be attributed to the fact that the surface coverage by $FeOH^+$ ions is much greater than the $NiOH^+$ surface coverage[10] which results in a smaller change in coverage due to presence of different concentrations of colloidal $SiO_2$ in the electrolyte. The hydrogen partial current density does not change significantly with the increase in the concentration of $SiO_2$.

Figure 12 represents the comparison between model predictions and experimental results for the weight fraction of $SiO_2$ in the deposit. At a fixed deposition potential, the amount of $SiO_2$ included increases as the concentration of $SiO_2$ in the solution is increased. The observed phenomena is probably due to the increased availability of $SiO_2$ particles in the solution in a colloidal form. The weight fraction

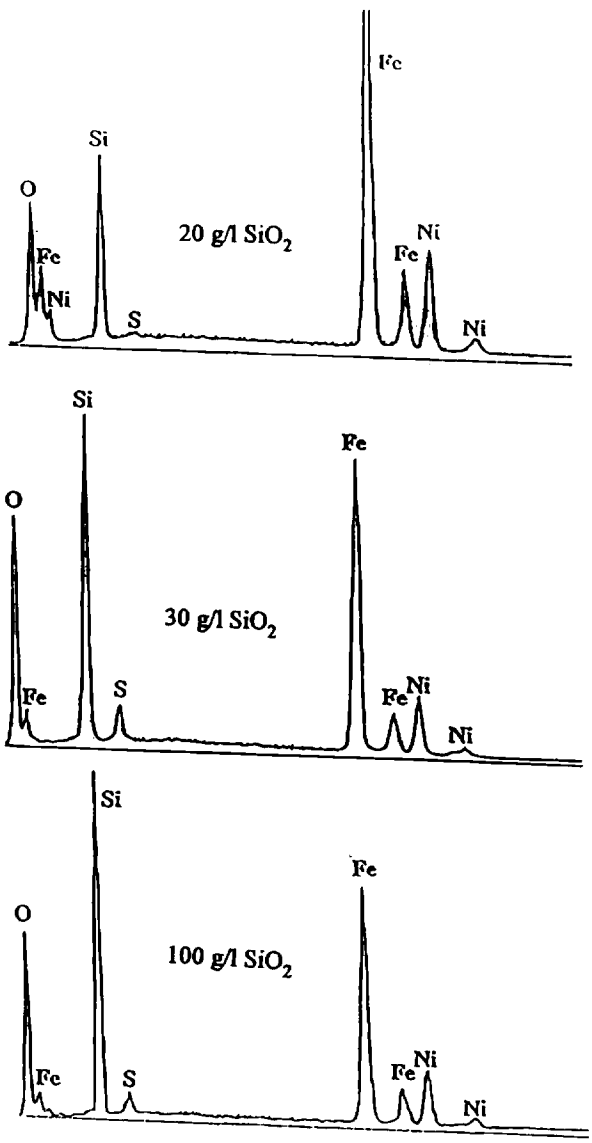


**Fig. 8. EDS spectra of deposits plated at −1.2 V *vs.* SCE with different concentrations of $SiO_2$ in solution.**

of colloid in the deposit decreased at more cathodic deposition potentials. The observed decrease in the weight fraction of $SiO_2$ was expected because a more cathodic deposition potential signifies a higher rate of deposition of nickel and iron at the electrode. However, for a given concentration of inert particles in the solution, the number of $SiO_2$ particles included was found to increase as the applied deposition potential was made more cathodic. This might be due to the following reason. At more cathodic deposition potentials, the rate of deposition of nickel and iron increases. This might result in a larger fraction of the adsorbed $SiO_2$ particles being incorporated. The increase in $SiO_2$ content with an increase in deposition potential to a more cathodic value is accounted for, in the model, by the potential dependent exponential term in Eq. 31.

## Conclusions

Experiments were carried out to characterize the electrodeposition of Fe-Ni alloy and Fe-Ni-$SiO_2$ composites. A mathematical model was developed which describes the material balance within the diffusion layer and predicts the adsorption phenomena for the potentiostatic elec-

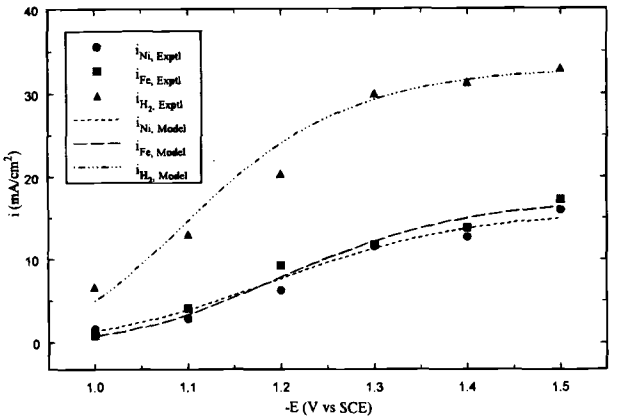


**Fig. 9. Comparison of model predictions and experimentally observed partial currents for Ni, Fe, and $H_2$ during deposition from a bath containing 3 g/liter $SiO_2$.**

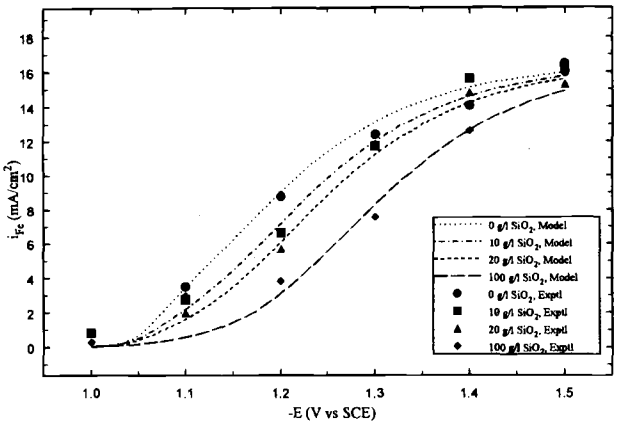


**Fig. 11. Model predictions for $i_{Fe}$ as a function of the applied potential for different concentrations of $SiO_2$ in solution.**

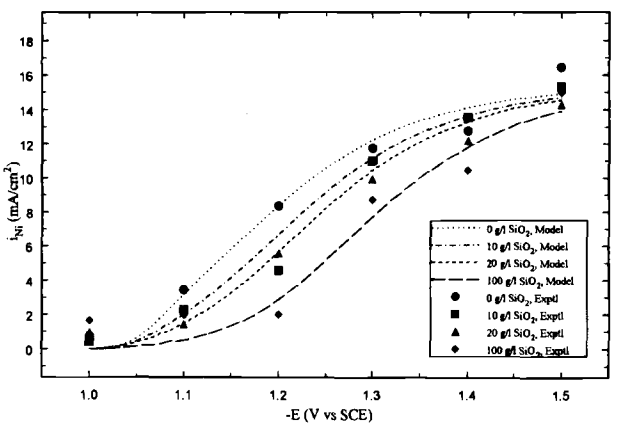


**Fig. 10. Model predictions for $i_{Ni}$ as a function of the applied potential for different concentrations of $SiO_2$ in solution.**

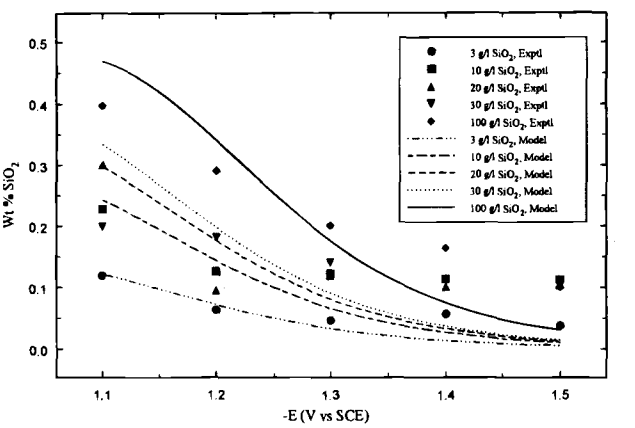


**Fig. 12. Plot of model predictions and experimental values obtained for the mass fraction of $SiO_2$ in the deposit for different concentrations of $SiO_2$ in solution.**

trodeposition of Fe-Ni alloys and Fe-Ni-$SiO_2$ composites. The model postulates the anomalous electrodeposition of Fe-Ni occurs through the adsorption and subsequent reduction of the metal monohydroxide ions ($FeOH^+$ and $NiOH^+$) only. The adsorption fraction of $FeOH^+$, $NiOH^+$, and $SiO_2$ is related to their respective interfacial concentration according to a Langmuir-type isotherm assuming that the uncovered surface is negligible compared to the covered surface. The predictions obtained using the model for the partial current densities for iron, nickel, and hydrogen for the content of the inert particle in the deposit agreed with the experimentally obtained profiles under potentiostatic conditions. Because of the surface coverage by $SiO_2$, the operating potential was extended in cathodic direction. Also, higher concentrations of electroactive species were predicted at the electrode surface which confines the surface reactions within the kinetically controlled region compared to the mass-transfer limitation in a bath without $SiO_2$. The weight fraction of $SiO_2$ in the deposit was found to increase with the increase of the concentration of $SiO_2$ in the electrolyte for deposition at a constant electrode potential. This resulted from the increase of the electrode surface coverage which is directly proportional to the concentration of $SiO_2$ in the electrolyte.

## Acknowledgment

Financial support by A. E. S. F. under Research Project RF-83 is gratefully acknowledged.

Manuscript submitted Oct. 10, 1995; revised manuscript received March 6, 1996.

*The University of South Carolina assisted in meeting the publication costs of this article.*

## LIST OF SYMBOLS

| | |
|---|---|
| $B$ | factor controlling potential dependent inclusion of inert particles, $V^{-1}$ |
| $c_i$ | concentration of species i, mol/cm³ |
| $c_{i,bulk}$ | bulk concentration of species i, mol/cm³ |
| $c_{i,o}$ | concentration of species i at the solid-solution interface, mol/cm³ |
| $d_{k,j}$ | density of species k that participates in reaction j, g/cm³ |
| $D_i$ | diffusion coefficient of species i, cm²/s |
| $E$ | applied electrode potential, V |
| $E_j^0$ | standard electrode potential of reaction j, V |
| $E_{e,j}$ | equilibrium potential corresponding to bulk concentrations for reaction j, V |
| F | Faraday's constant, 96,487 C/mol |
| $i_j$ | partial current density due to reaction j, A/cm² |
| $i_{oj}$ | exchange current density of reaction j, A/cm² |
| $k_i$ | relative adsorption equilibrium constant of inert particle i to metal hydroxide ion |
| $K_i$ | equilibrium constant of chemical reaction i |
| $M_i^{z_i}$ | symbol for species i with charge $z_i$ |
| $n_j$ | number of electrons transferred in reaction j |
| $N_i$ | flux of species i, mol/cm² s |
| $Q$ | charge removed during the anodic sweep cycle, C |
| $R$ | universal gas constant, 8.3143 J/mol-K |
| $R_i$ | rate of generation of species i, mol/cm³ s |
| $s_{i,j}$ | stoichiometric coefficient of ionic species i in reaction j |
| T | absolute temperature, K |
| $v_i$ | volume of species i in solid phase per unit area, cm³/cm² |
| $v_0$ | measure of the factor of inclusion caused by adsorption, cm/s |

$v_y$ velocity of the electrolyte in the direction of the normal coordinate $y$, cm/s
$V_d$ potential of the working electrode, V
$w_{kj}$ atomic weight of metal k that is involved in electrochemical reaction j, g/mol
$X_i$ weight fraction of metal i given as (weight of metal i/total weight of material deposited)
$y$ normal coordinate, cm
$z_i$ charge number of species i

Greek

$\alpha_i$ volume fraction of inert particle i in the deposit
$\alpha_{a,j}$ anodic transfer coefficient for reaction j
$\alpha_{c,j}$ cathodic transfer coefficients for reaction j
$\eta_{j,ref}$ electrode overpotential with respect to a reference open-circuit potential, (bulk concentration is chosen as the reference state), V
$\theta_i$ surface coverage fraction of i
$\lambda_i$ absolute activity of ionic species i
$\Phi$ solution potential, V
$\Phi_0$ solution potential at interface, V

Subscripts

e equilibrium value
i ionic species
j electrochemical reaction j
k metal k deposited during an electrochemical reaction

Superscripts

nr total number of electrochemical reactions

## REFERENCES


1. H. Dahms, *J. Electroanal. Chem., Interfacial Electrochem.*, **8**, 5 (1964).
2. H. Dahms and I. M. Croll, *This Journal*, **112**, 771 (1965).
3. I. M. Croll and L. T. Romankiw, in *Electrodeposition Technology, Theory and Practice*, L. T. Romankiw and D. R. Turner, Editors, PV 87-17, p. 285, The Electrochemical Society Proceedings Series, Pennington, NJ (1987).
4. M. J. Nicol and H. I. Philip, *J. Electroanal. Chem., Interfacial Electrochem.*, **70**, 233 (1976).
5. S. Swathirajan, *This Journal*, **133**, 671 (1986).
6. J. O'M. Bockris, D. Drazic, and A. R. Despic, *Electrochim. Acta*, **4**, 325 (1961).
7. J. Matulis and R. Slizys, *ibid.*, **9**, 1177 (1964).
8. S. Hessami and C. W. Tobias, *This Journal*, **136**, 3611 (1989).
9. W. C. Grande and J. B. Talbot, *ibid.*, **140**, 669 (1992).
10. M. Matlosz, *ibid.*, **140**, 2272 (1993).
11. N. Guglielmi, *ibid.*, **119**, 1009 (1972).
12. M. Van Camp, Engineering Thesis, Katholieke Universiteit, Leuven, Belgium (1979).
13. E. P. Rajiv and S. K. Seshadri, *Plat. Surf. Finish.*, **10**, 66 (1993).
14. P. W. Wild, *Modern Analysis for Electroplating*, **A-15**, Finishing Publications, Hampton Hill (1974).
15. P. H. Reiger, *Electrochemistry*, 2nd ed., p. 331-336, Chapman and Hall, New York (1991).
16. J. S. Newman, *Electrochemical Systems*, Prentice-Hall, Englewood Cliffs, NJ (1991).
17. R. E. White, *Ind. Eng. Chem. Fundam.*, **17**, 367 (1978).
18. J. C. Whithers, *Prod. Fin.*, **8** (1962).
19. P. W. Martin and R. V. Williams, in *Proceedings of Interfinish '64*, pp. 182-188, British Iron and Steel Research Assoc., London (1964).
20. E. A. Brandes and D. Golthorpe, *Metallurgica*, **1**, 195 (1967).
21. A. M. J. Kariapper and J. Foster, *Trans Inst. Met. Finish.*, **52**, 87 (1974).
22. J. P. Celis, J. R. Roos, and C. Buelens, *This Journal*, **134**, 1402, (1987).
23. J. L. Valdes, *ibid.*, **134**, 223C (1987).
24. J. Fransaer, J. P. Celis, and J. R. Roos, *ibid.*, **139**, 413 (1992).
25. K.-M. Yin, J. H. Wei, J.-R. Fu, B. N. Popov, S. N. Popova, and R. E. White, *J. Appl. Electrochem.*, **25**, 543 (1995).
26. B. N. Popov, K.-M. Yin, and R. E. White, *This Journal*, **140**, 1321 (1993).
27. B. N. Popov, S. N. Popova, K.-M. Yin, and R. E. White, *Plat. Surf. Fin.*, **81**, 65 (1994).
28. D. J. Pickett, *Electrochemical Reactor Design*, Elsevier, New York (1977).
29. *CRC Handbook of Chemistry and Physics*, 59th ed., R. C. Weast, Editor, CRC Press, Inc., Boca Raton, FL (1978-79).
30. U. Landau, in *Electrodeposition Technology, Theory, and Practice*, L. T. Romankiw and D. R. Turner, Editors, PV 87-17, p. 589, The Electrochemical Society Proceedings Series, Pennington, NJ (1987).